

# Mechanistic Basis of OXA-48-like $\beta$ -lactamases Hydrolysis of Carbapenems

Vlatko Stojanoski<sup>1,2</sup>, Liya Hu<sup>1</sup>, Banumathi Sankaran<sup>3</sup>, Feng Wang<sup>4</sup>, Peng Tao<sup>4</sup>, B.V. Venkataram Prasad<sup>1</sup>, and Timothy Palzkill<sup>\*1,2</sup>

From the <sup>1</sup>Verna and Marrs McLean Department of Biochemistry and Molecular Biology and <sup>2</sup>Department of Pharmacology and Chemical Biology, Baylor College of Medicine, Houston, TX, USA, <sup>3</sup>Department of Molecular Biophysics and Integrated Bioimaging, Berkeley Center for Structural Biology, Lawrence Berkeley National Laboratory, Berkeley, CA, USA, <sup>4</sup>Department of Chemistry, Center for Research Computing, Center for Drug Discovery, Design, and Delivery (CD4), Southern Methodist University, Dallas, TX, USA

\* Corresponding Author: Timothy Palzkill, Department of Pharmacology and Chemical Biology, Baylor College of Medicine, One Baylor Plaza, Houston, TX 77030, USA, Tel:(713) 798-5609; E-mail: timothyp@bcm.edu

**KEYWORDS:** *Antibiotic resistance, carbapenems, serine  $\beta$ -lactamases, OXA-enzymes, carbapenemases, OXA-48-like enzymes.*

Running Title: Carbapenem hydrolysis by OXA-48-like  $\beta$ -lactamases

**Abstract**

Carbapenem-hydrolyzing class D  $\beta$ -lactamases (CHDLs) are an important source of resistance to these last resort  $\beta$ -lactam antibiotics. OXA-48 is a member of a group of CHDLs named OXA-48-like enzymes. Based on sequence similarity, OXA-163 can be classified as an OXA-48-like enzyme but it has altered substrate specificity. Compared to OXA-48, it shows impaired activity for carbapenems but displays enhanced hydrolysis of oxyimino-cephalosporins. Here, we address the mechanistic and structural basis for carbapenem hydrolysis by OXA-48-like enzymes. Pre-steady state kinetic analysis indicates that the rate-limiting step for OXA-48 and OXA-163 hydrolysis of carbapenems is deacylation and that the greatly reduced carbapenemase activity of OXA-163 compared to OXA-48 is due entirely to a slower deacylation reaction. Furthermore, our structural data indicate that the positioning of the  $\beta$ 5- $\beta$ 6 loop is necessary for carbapenem hydrolysis by OXA-48. A major difference between the OXA-48 and OXA-163 complexes with carbapenems is that the 214-RIEP-217 deletion in OXA-163 creates a large opening in the active site that is absent in the OXA-48/carbapenem structures. We propose the larger active site results in less constraint on the conformation of the 6 $\alpha$ -hydroxyethyl group in the acyl-enzyme. The acyl-enzyme intermediate assumes multiple conformations, most of which are incompatible with rapid deacylation. Consistent with this hypothesis, molecular dynamics simulations indicate the most stable complex is formed between OXA-48 and imipenem, which correlates with the OXA-48 hydrolysis of imipenem being the fastest observed. Further, the OXA-163 complexes with imipenem and meropenem are the least stable and show significant conformational fluctuations, which correlates with the slow hydrolysis of these substrates.

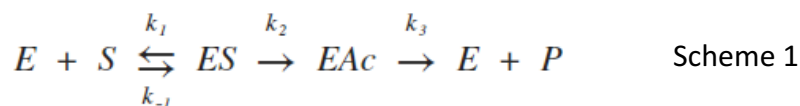
## Introduction

Antibiotic resistance is a worldwide problem that is growing at an alarming rate<sup>1-3</sup>. An increasing number of bacterial infections acquired in hospital settings are caused by carbapenem-resistant *Enterobacteriaceae* (CRE) pathogens<sup>4-6</sup>. The major causative agents of CRE infections are bacterial species belonging to the Gram-negative bacilli *Klebsiella*, with *Klebsiella pneumoniae* representing 80% of these infections<sup>7-10</sup>. Resistance to carbapenems is a concern in that these drugs have a broad spectrum of activity, high potency, and are used as last resort  $\beta$ -lactam antibiotics for infections with pathogens resistant to earlier generation antibiotics<sup>11-13</sup>.

*Klebsiella pneumoniae* frequently become resistant to carbapenem antibiotics by acquiring plasmid-encoded  $\beta$ -lactamases named carbapenemases<sup>14,15</sup>.  $\beta$ -lactamases are grouped into four classes (A-D) based on primary amino acid sequence homology. Classes A, C, and D are serine hydrolases while class B consists of zinc metallo-enzymes<sup>16,17</sup>. Carbapenemases found in *K. pneumoniae* belong to either metallo- (class B) or serine  $\beta$ -lactamase (classes A and D) classes<sup>18</sup>. The three most frequently encountered carbapenemases in clinics worldwide are KPC (class A), OXA-48 (class D), and NDM (class B)<sup>18-20</sup>.

OXA-48 was first isolated more than a decade ago from a nosocomial infection with *K. pneumoniae* in Turkey and since then has disseminated worldwide<sup>21</sup>. OXA-48 is a carbapenem-hydrolyzing, class D,  $\beta$ -lactamase (CHDL). Among all class D enzymes, it has the highest catalytic efficiency ( $k_{cat}/K_m$ ) for hydrolysis of the carbapenem imipenem<sup>19,22</sup>. OXA-48 is a member of a subgroup of class D enzymes termed OXA-48-like enzymes, which includes 12 enzymes differing from OXA-48 by one to five amino acids<sup>23,24</sup>. Most enzymes in the OXA-48-like group have very similar carbapenemase profiles<sup>19,24</sup>. Exceptions to this are OXA-163, OXA-247, and OXA-405, which are grouped with OXA-48-like enzymes by sequence homology yet display poor carbapenemase activity<sup>23-25</sup>. Previous reports show that OXA-48 and OXA-163 also have very different catalytic efficiency for the hydrolysis of other  $\beta$ -lactam antibiotics such as oxyiminocephalosporins<sup>24,26</sup>. OXA-163, similarly to OXA-48, was isolated in the clinic from an infection of *K. pneumoniae*, but it differs from OXA-48 by one substitution, S212D, and a four-amino acid deletion, 214-RIEP-217<sup>26</sup>. The sequence changes in OXA-163 eliminate the bottom boundary of the active site causing an expansion of the active-site cavity<sup>27</sup> (Fig. 1).

Class D  $\beta$ -lactamases such as OXA-48 are serine hydrolases with a mechanism similar to serine proteases. After formation of the enzyme-substrate complex (ES), the active-site serine attacks and forms a covalent, acyl-enzyme intermediate (EAc)<sup>28</sup>. Subsequent activation of a water molecule and hydrolysis of the acyl-enzyme generates the hydrolyzed product (P)(Scheme 1), which is inactive as an antibiotic. In class D enzymes, the deacylation water is activated by a carboxylated lysine<sup>29</sup>.



Unlike the OXA-48-like enzymes, most class D  $\beta$ -lactamases are inhibited by carbapenems via formation of a long-lived, covalent acyl-enzyme complex<sup>12</sup>. For these enzymes, nucleophilic attack by the catalytic Ser70 to form the acyl-enzyme occurs rapidly, but deacylation by water to the hydrolyzed product occurs very slowly. Carbapenems are thought to be poor substrates for  $\beta$ -lactamases due to the presence of the pyrroline ring adjacent to the  $\beta$ -lactam ring as well as the small R1 6 $\alpha$ -hydroxyethyl moiety<sup>30-32</sup>. Several mechanisms have been proposed to explain the poor hydrolysis of carbapenems by serine active site  $\beta$ -lactamases. First, the pyrroline ring can undergo tautomerization upon the acylation by the catalytic serine, which produces two isomers,  $\Delta^1$  and  $\Delta^2$  (Fig. S1). The  $\Delta^2$  isomer has been suggested to be more favorable for subsequent deacylation and hydrolysis<sup>33,34</sup>. Second, the 6 $\alpha$ -hydroxyethyl group forms a hydrogen bond with the deacylating water and reduces its nucleophilicity, thereby slowing the deacylation rate<sup>30</sup>. In contrast, the SFC-1 class A carbapenemase constrains the position of the hydroxyethyl group away from the water, which is suggested to enhance nucleophilicity of the water leading to a faster deacylation rate<sup>32</sup>. Finally, structures of the non-carbapenemase TEM-1 and SHV-1 class A  $\beta$ -lactamases acylated by imipenem and meropenem, respectively, reveal a conformational change of the acylated substrate whereby the carbonyl oxygen of the  $\beta$ -lactam ring is no longer in the oxyanion hole - thereby blocking the deacylation reaction<sup>30,31</sup>.

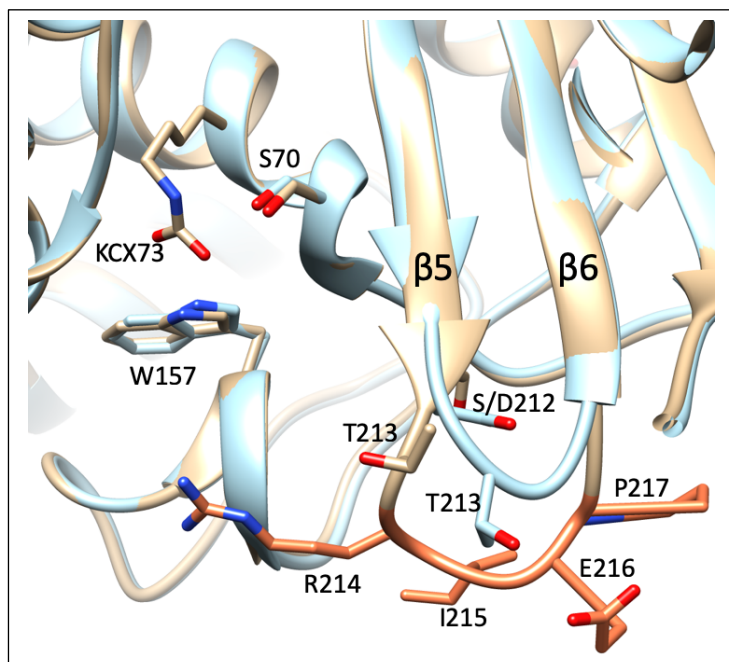


**Figure 1.** Overlay of OXA-48 (tan) and OXA-163 (light blue) outlining the active site cavity. In the center is the S70 nucleophile, to the left of the serine is the N-carboxylated K73 general base, which is coordinated in part by W157. Represented in orange stick model are the four residues

deleted in OXA-163. The important elements outlining the active site are labeled. The active site is confined between the  $\beta$ 5-strand on the right and the bottom in OXA-48 by R214. In OXA-163, the absence of R214 extends the active site by eliminating the bottom boundary.

In class D  $\beta$ -lactamases additional factors interfere with carbapenem hydrolysis. The 6 $\alpha$ -hydroxyethyl group obstructs access for a water molecule to be activated by the carboxylated lysine and attack the carbonyl carbon of the acyl-enzyme<sup>35,36</sup>. To explain how a nucleophilic water gains access to the acyl enzyme in OXA-23 and OXA-143 it has been proposed that movement of either a conserved active site leucine or valine opens a channel for the water molecule to reach the catalytic lysine to promote deacylation<sup>35</sup>. It has also been suggested, based on X-ray structures and molecular dynamics simulations, that rotation of a carbapenem in the active site of OXA-48 may allow access of a water molecule to a position consistent with deacylation<sup>22,36</sup>.

Due to the high clinical relevance, there have been several recent structural studies on the mechanism of carbapenem hydrolysis by OXA-48<sup>36-38</sup>. However, the acylation and deacylation rate constants for carbapenem hydrolysis by OXA-48 are not known and the mechanism(s) behind the decrease in carbapenem hydrolysis by the OXA-163 enzyme has not been addressed. To investigate the mechanism of carbapenem hydrolysis mediated by OXA-48 and OXA-163, pre-steady kinetic studies were performed for imipenem and meropenem, revealing that deacylation of the acyl-enzyme intermediate is the rate-limiting step for both enzymes for both substrates. However, compared to OXA-48, OXA-163 has a greatly decreased deacylation rate that results in the slow hydrolysis of carbapenems.

To gain further insight into the structural basis of the different substrate profiles of OXA-48 and OXA-163 and more generally about the basis of the high carbapenemase activity of OXA-48-like enzymes, we determined the structures of the acyl-enzyme intermediates of these enzymes with imipenem and meropenem. The structures show in all cases that the acylated carbapenem is in the  $\Delta^2$  tautomeric form and that the carbonyl oxygen originating from the  $\beta$ -lactam ring is positioned in the oxyanion hole. These findings are consistent with efficient deacylation. Thus, tautomerization and the occupancy of the oxyanion hole cannot explain the differences in catalysis/specificity between OXA-48 and OXA-163. Further, the hydroxyl group from the 6 $\alpha$ -hydroxyethyl moiety is directed away from the carboxylated lysine and deacylation water for both carbapenems in the OXA-48 and OXA-163 structures, suggesting it does not play a role in the slow deacylation of carbapenems by these enzymes. A major difference between the OXA-48 and OXA-163 complexes with carbapenems is the 214-RIEP-217 deletion in OXA-163, which creates a large opening in the active site that is absent in the OXA-48/carbapenem structures. We propose the larger active site results in less constraint on the conformation of the 6 $\alpha$ -hydroxyethyl group in the acyl-enzyme, which allows the intermediate to assume multiple non-productive conformations that would slow deacylation. Finally, molecular dynamics simulation studies of complexes of OXA-48 and OXA-163 with imipenem and meropenem indicate the most stable complex is formed between OXA-48 and imipenem, which correlates with the OXA-48 hydrolysis of imipenem being the fastest observed. The OXA-163 complexes with imipenem and meropenem are also less stable and show significant conformational fluctuations

compared to complexes with OXA-48, which correlates with the slow hydrolysis of these substrates by OXA-163.

## Results

### *Carbapenem turnover is reduced in OXA-163 versus OXA-48*

Non-carbapenemase class D  $\beta$ -lactamases hydrolyze carbapenems poorly due to a very slow deacylation rate. OXA-48 hydrolyzes carbapenems more rapidly, but the rate-limiting step of this reaction is not known. OXA-163 is an OXA-48-like variant that hydrolyzes carbapenems slowly but the kinetic basis for the slower rate is not known.

In order to examine the kinetics of carbapenem hydrolysis, steady-state kinetics experiments were performed with imipenem and meropenem as substrates (Table 1). OXA-48 displays a 28-fold higher turnover rate ( $k_{cat}$ ) for hydrolysis of imipenem compared to meropenem, consistent with the observation that several CHDL enzymes hydrolyze imipenem faster than meropenem<sup>24,27,39,40</sup>. In the  $\beta$ -lactamase kinetic scheme,  $k_{cat}$  reflects the magnitude and relationship between the acylation ( $k_2$ ) and deacylation ( $k_3$ ) rates<sup>41,42</sup> and, therefore, the 28-fold increased turnover of imipenem reflects higher  $k_2$  and/or  $k_3$  values compared to meropenem. Similarly, the  $k_{cat}/K_M$  value for imipenem hydrolysis by OXA-48 is 45-fold higher than that for meropenem. In the  $\beta$ -lactamase kinetic scheme,  $k_{cat}/K_M$  reflects the rates up to the formation of the acyl-enzyme, and therefore indicates increased binding affinity ( $K_D$ ) and/or a faster acylation rate ( $k_2$ ) for imipenem versus meropenem for OXA-48. Finally, the  $K_M$  value for both imipenem and meropenem hydrolysis by OXA-48 is very low (<5  $\mu$ M). It was not possible to accurately determine the values because of the low substrate concentrations involved (Table 1).  $K_M$  is a complex term in the  $\beta$ -lactamase kinetic scheme and does not necessarily reflect substrate binding affinity in that a strongly limiting deacylation rate ( $k_3$ ) can also lead to low  $K_M$  values<sup>41,42</sup>.

**Table 1.** Kinetic parameters of OXA-48 and OXA-163.

Enzyme	Substrate	
	Imipenem	Meropenem
<b>OXA-48</b>		
$k_{cat}$ ( $s^{-1}$ )	$2.8 \pm 0.2$	$0.1 \pm 0.01$
$K_m$ ( $\mu$ M)	$\leq 3.0 \pm 0.6$	$\leq 5.0 \pm 1.5$
$k_{cat}/K_m$ ( $M^{-1}s^{-1}$ )	$9.1 \times 10^5$	$2.0 \times 10^4$
$k_2$ ( $s^{-1}$ )	$86 \pm 12$	$300 \pm 28$
$k_3$ ( $s^{-1}$ )	$3.0^a \pm 1.1$	$0.15 \pm 0.01$
$K_s'$ ( $\mu$ M)	$98 \pm 32$	$129 \pm 31$
<b>OXA-163</b>		
$k_{cat}$ ( $s^{-1}$ )	$0.005 \pm 0.001$	$0.022 \pm 0.002$
$K_m$ ( $\mu$ M)	$\leq 3.8 \pm 1$	$5.6 \pm 0.5$
$k_{cat}/K_m$ ( $s^{-1}M^{-1}$ )	$1.3 \times 10^3$	$3.9 \times 10^3$
$k_2$ ( $s^{-1}$ )	$250 \pm 19$	$95 \pm 7$
$k_3$ ( $s^{-1}$ )	$0.011 \pm 0.005$	$0.031 \pm 0.011$

$K_s'$ ( $\mu\text{M}$ )	$92 \pm 22$	$21 \pm 5$
--------------------------	-------------	------------

<sup>a</sup> This rate constant was determined using equation 3. The error on the calculated  $k_3$  value was determined by propagating the error on  $k_{\text{cat}}$  and  $k_2$  (Materials and Methods).

OXA-48, like most other family members, is a good catalyst of carbapenem hydrolysis, although imipenem is a 30-fold better substrate than meropenem. In comparison to OXA-48, OXA-163 has lost considerable activity (about 500-fold decrease in  $k_{\text{cat}}$ ) for imipenem hydrolysis and has somewhat less activity against meropenem (five-fold) (Table 1). This result is opposite to the characteristic CHBL profile that is observed for OXA-48<sup>27</sup>. Because  $k_{\text{cat}}$  is reduced,  $k_2$  and/or  $k_3$  must be slower for imipenem and meropenem catalysis by OXA-163 compared to OXA-48. Therefore, the four amino acid deletion and S212D substitution present in OXA-163 relative to OXA-48 results in a decrease in carbapenem turnover, particularly for imipenem.

The  $k_{\text{cat}}/K_M$  value for imipenem hydrolysis by OXA-163 is nearly 1000-fold lower than that for OXA-48 while that for meropenem is 5-fold lower than OXA-48. This result indicates that substrate binding affinity ( $K_D$ ) and/or the acylation rate are reduced by the four amino acid deletion and S212D substitution present in OXA-163 relative to OXA-48. As with OXA-48, the  $K_M$  values for carbapenem hydrolysis by OXA-163 are very low with both imipenem and meropenem as substrate (Table 1). Consequently, it was not possible to directly determine the  $K_M$  because of the low substrate concentrations that would be required. As noted above, a low  $K_M$  does not necessarily reflect tight substrate binding as rate-limiting deacylation can lead to  $K_M$  values below the  $K_D$  for substrate.

#### *Carbapenem deacylation is rate-limiting for OXA-48 and strongly rate-limiting for OXA-163*

The steady-state kinetic parameters for both imipenem and meropenem hydrolysis indicate a large decrease in  $k_{\text{cat}}$  for OXA-163 compared to OXA-48 (Table 1). Since the  $\beta$ -lactam hydrolysis reaction consists of two distinct steps (acylation and deacylation) as outlined in Scheme 1, the  $k_{\text{cat}}$  value is constrained by the rate-limiting step, which in the case of serine  $\beta$ -lactamases may be acylation, deacylation, or both if the rates are similar<sup>41,43,44</sup>. The steady-state kinetic data do not allow the determination of the rate-limiting step(s) in carbapenem hydrolysis for either enzyme. Consequently, the individual acylation ( $k_2$ ) and deacylation ( $k_3$ ) rate constants were determined experimentally for both enzymes using pre-steady-state kinetics and recovery of enzymatic activity assays, respectively<sup>45,46</sup>.

The acylation rate constants for imipenem and meropenem were determined by stopped-flow kinetics under single turnover conditions with enzyme in excess<sup>45,47</sup> (Table 1, Fig. 2). OXA-48 and OXA-163 were found to have similar acylation rate constants (less than 3-fold difference) for both carbapenems. In the case of imipenem, the  $k_2$  values were much larger than the corresponding  $k_{\text{cat}}$  values (30-fold for OXA-48 and 50,000-fold for OXA-163) indicating that acylation is not the rate-limiting step for imipenem hydrolysis by either enzyme. The acylation rate constants for meropenem hydrolysis were also much higher than the corresponding  $k_{\text{cat}}$  values (3,000-fold for OXA-48 and 4,300-fold for OXA-163) indicating acylation is not rate limiting, even with a poorer substrate. Overall, the acylation rate constants for imipenem and meropenem hydrolysis by OXA-48 and OXA-

163 indicate that both enzymes acylate these carbapenem substrates relatively rapidly and at similar rates.

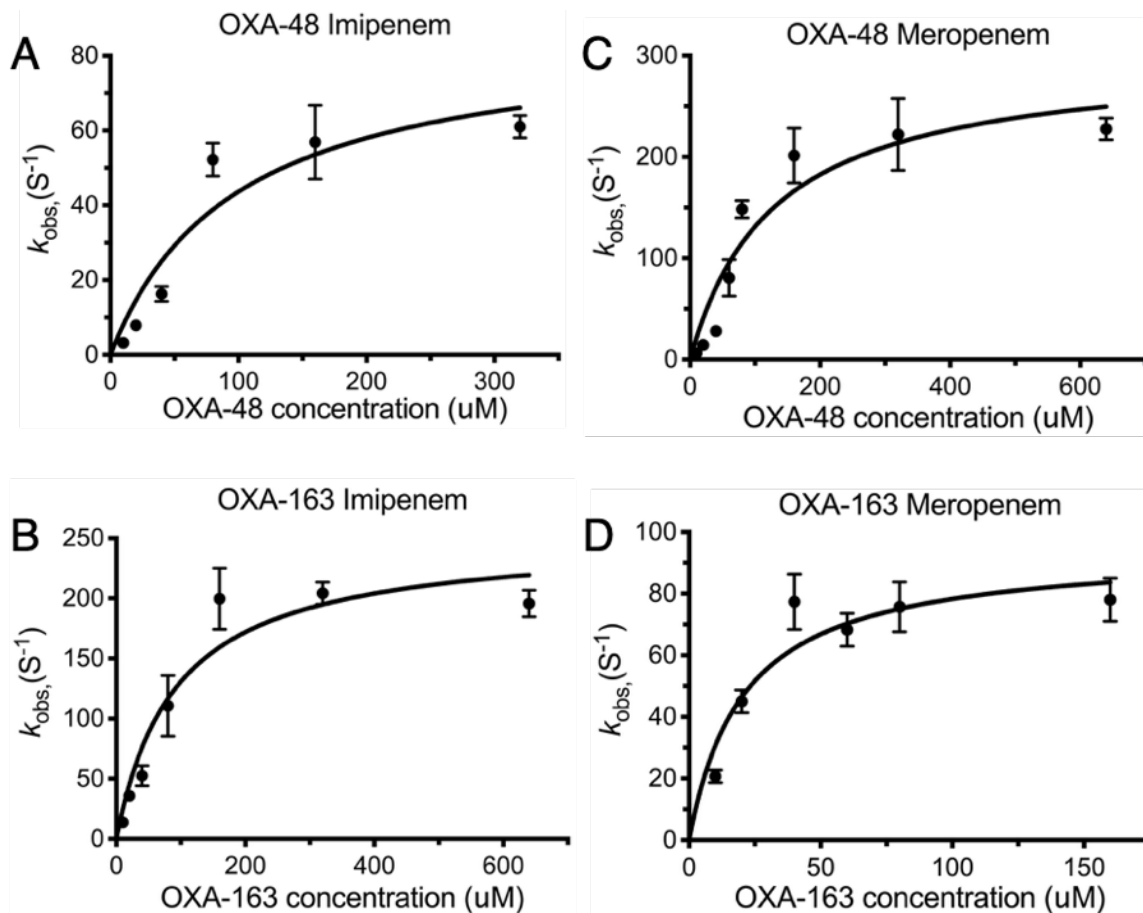


**Figure 2.** Determination of  $k_2$  based on fits of the apparent constants ( $k_{obs}$ ) obtained using single-turnover kinetics for OXA-48 and OXA-163 with imipenem and meropenem. **A.** and **C.**  $k_{obs}$  values of OXA-48 for imipenem and meropenem, respectively. **B.** and **D.** Determination of  $k_2$  based on fits of  $k_{obs}$  values of OXA-163 for imipenem and meropenem, respectively. Acylation constants were determined using equation 1.

In order to test the hypothesis that deacylation is rate-limiting for the hydrolysis of imipenem and meropenem by OXA-48 and OXA-163, the deacylation rate constants ( $k_3$ ) were determined directly using the enzyme reactivation method<sup>46</sup>. Progress curves of hydrolysis of the colorimetric substrate nitrocefin revealed the reactivation rate of OXA-48 and OXA-163 after incubation with imipenem and meropenem (Fig. 3, Table 1). In all cases, the deacylation rate constants ( $k_3$ ) were much lower than the rate constants observed for acylation and were comparable to the corresponding  $k_{cat}$  values (Table 1). This confirms that deacylation is the rate-limiting step for carbapenem hydrolysis by both OXA-48 and OXA-163. The deacylation rate of imipenem by OXA-48 could not be measured accurately by the reactivation method because of fast recovery due to a relatively high  $k_{cat}$  value (Fig. 3, Table 1). As a result, the  $k_3$  for OXA-48 with imipenem was

obtained with Equation 4 using the experimentally determined  $k_{\text{cat}}$  and  $k_2$  values. This calculation yields a  $k_3$  of  $3.0 \text{ s}^{-1}$  for OXA-48 with imipenem, which is almost identical to the  $k_{\text{cat}}$  of  $2.8 \text{ s}^{-1}$ , indicating that the rate-limiting step is deacylation. The OXA-48 deacylation rate constant for imipenem was 20-fold higher than that for meropenem. Thus, meropenem is turned over more slowly by OXA-48 compared to imipenem due to slower deacylation. Moreover, the  $k_3$  values of OXA-48 for imipenem and meropenem are higher than the  $k_3$  values of OXA-163 by 270-fold and 5-fold, respectively. Therefore, OXA-163 is a poor carbapenemase compared to OXA-48 because of slower deacylation rates.

In summary, the kinetics results indicate that the rate-limiting step for hydrolysis of both imipenem and meropenem by the OXA-48 carbapenemase is deacylation. In addition, the slower hydrolysis of meropenem versus imipenem by OXA-48 can be attributed to the much slower deacylation of meropenem. Finally, the S212D substitution and 214-RIEP-217 deletion in OXA-163 relative to OXA-48 further perturbs the deacylation step, leading to a large decrease in the turnover rate compared to OXA-48. This is especially pronounced in the case of imipenem. The deacylation rate constant for meropenem is less affected by the structural changes between OXA-48 and OXA-163.

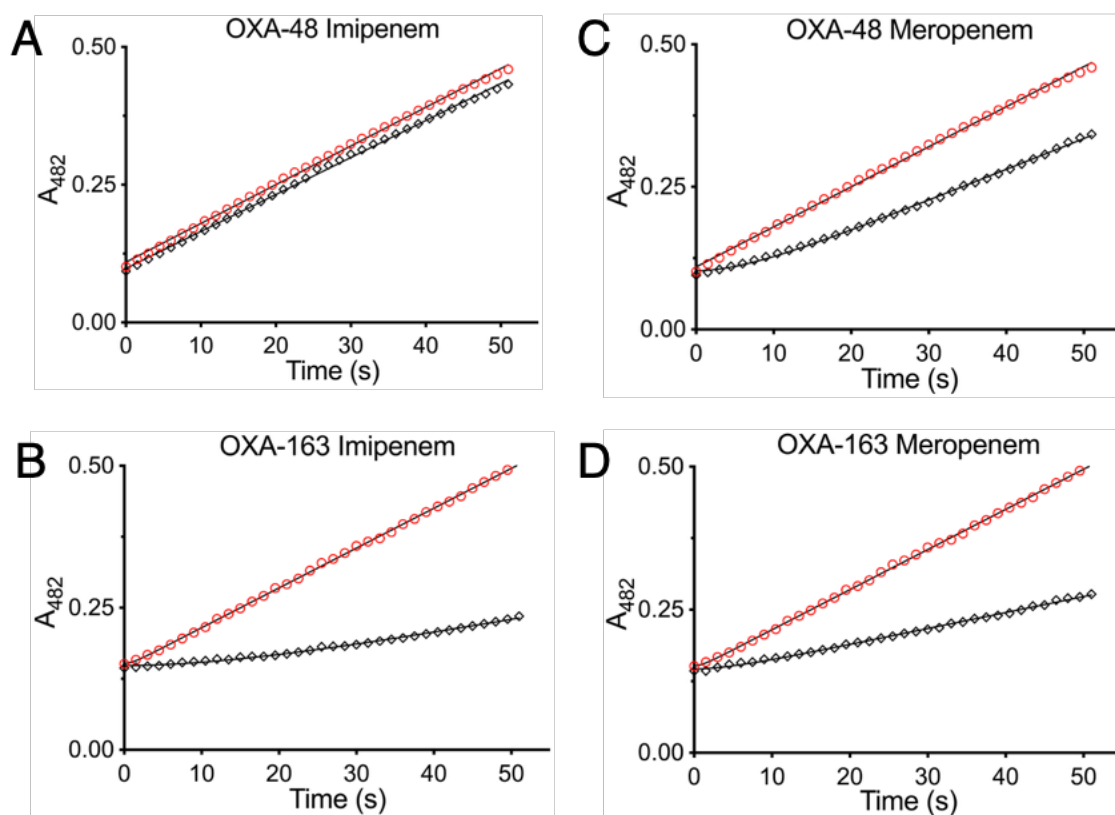


**Figure 3.** Reactivation of OXA-48 and OXA-163 after incubation with imipenem and meropenem. **A.** and **C.** Progress curves and fits of OXA-48 nitrocefin hydrolysis after incubation with imipenem and meropenem. **B.** and **D.** Progress curves and fits of OXA-163 nitrocefin hydrolysis after incubation with imipenem and meropenem, respectively. The red circles show the control condition of nitrocefin hydrolysis in the absence of incubation with carbapenem. The black

diamonds show the experimental condition of nitrocefin hydrolysis after incubation with carbapenem. The black lines are the fits of the data to equation 3 (Materials and Methods).

*X-ray structures of OXA-48 K73A mutant reveal similar conformations of carbapenems in the active site*

Having determined that deacylation is rate limiting for carbapenem hydrolysis by both OXA-48 and OXA-163, we next determined the X-ray structures of deacylation-deficient K73A mutants of OXA-48 and OXA-163 in complex with imipenem and meropenem to investigate the structural differences that contribute to the observed deacylation rates. K73A mutants were used to prevent substrate turnover since the wild-type enzymes hydrolyze the  $\beta$ -lactam ring and release the inactivated product. Previously, K73A mutants have been used successfully to determine the structure of the acyl-enzyme complex of OXA-enzymes with  $\beta$ -lactam antibiotics<sup>48</sup>.

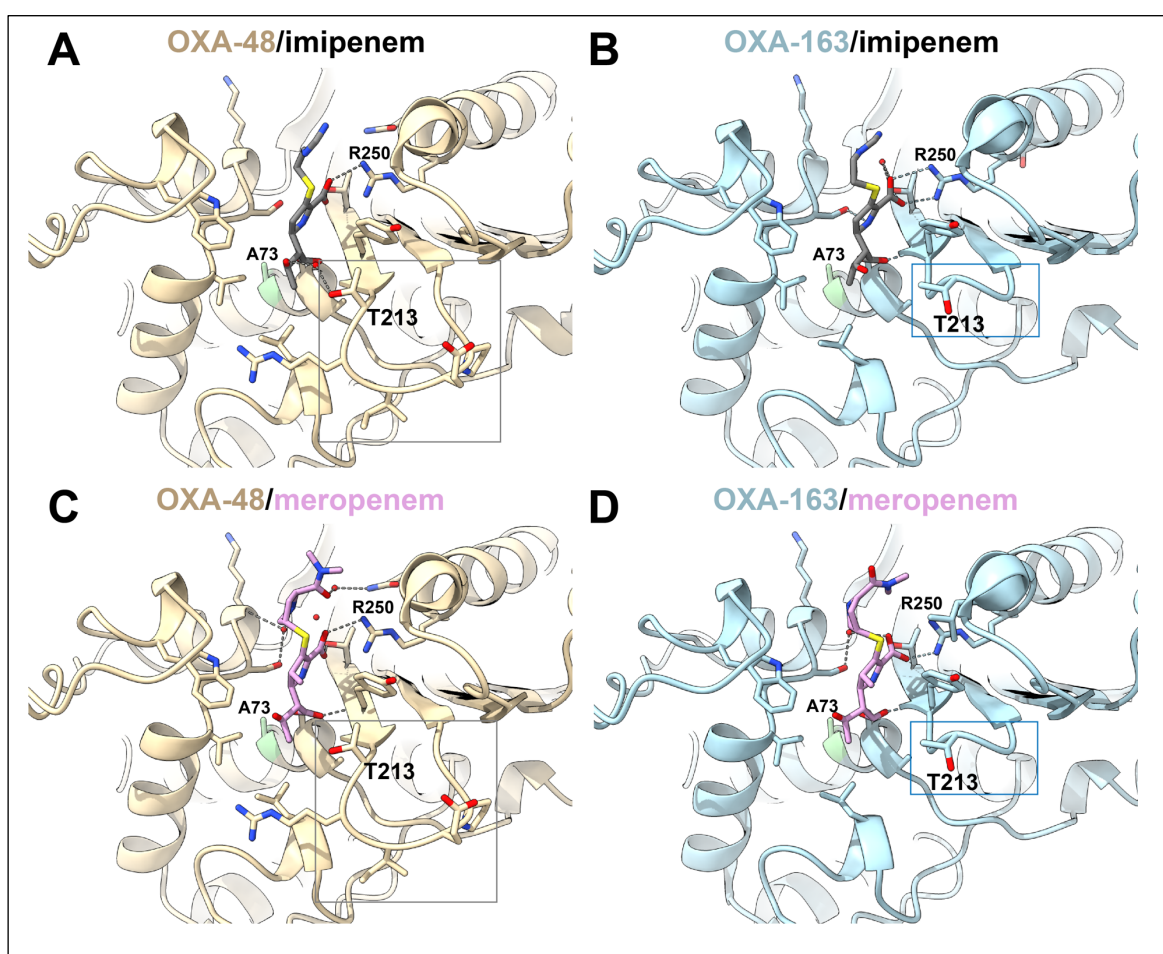


**Figure 4.** Schematic of the structures of the OXA-48 K73A and OXA-163 K73A acyl-enzyme complexes with imipenem and meropenem. **A.** Active-site region of the OXA-48 K73A enzyme with Ser70 forming a covalent acyl-enzyme with imipenem. The  $\beta$ 5- $\beta$ 6 loop containing Thr213 that constrains the size of the active site is indicated in the boxed region. Hydrogen bonds are shown as dotted black lines. Carbon atoms are shown in tan, oxygen in red, nitrogen in blue, and sulfur in yellow. Imipenem carbon atoms are shown in gray. **B.** Active-site region of the OXA-163



The crystal structure of OXA-48 K73A bound to imipenem was determined at 2.3 Å resolution (Table 2). The structure crystallized with two molecules in the asymmetric unit in the P22<sub>1</sub>2<sub>1</sub> space group. Strong residual electron density in the F<sub>o</sub> - F<sub>c</sub> simulated annealing omit difference maps indicated the presence of imipenem attached to the O<sub>γ</sub> of Ser70 in both chains. The two chains in the asymmetric unit are superimposable and the covalently attached imipenem also shows a very similar structure with minor differences in the extended, flexible C2 substituent (Fig. S2). Hydrogen bonds constituting the oxyanion hole occur between the -NH main chain atoms of Ser70 and Tyr211 and the C7 acyl-carbonyl oxygen of imipenem (Figs. 4A, 5). Also, the C3 carboxyl group of imipenem makes hydrogen bonding interactions with the side chains of Thr209 and Arg250 (Figs. 4A, 5). Previous structures of OXA-48 with acylated imipenem have revealed two tautomers of the pyrroline ring<sup>36,38</sup>. In the Δ<sup>1</sup> tautomer, the C2 atom of the pyrroline ring is sp<sup>3</sup> hybridized, while the Δ<sup>2</sup> state has C2 in a planar configuration indicating sp<sup>2</sup>-hybridization. Both chains of the OXA-48 K73A/imipenem structure display the Δ<sup>2</sup> tautomeric state (Fig. 4A). The hydroxyethyl group of imipenem is in a similar position and conformation as observed in previous OXA-48 acyl-enzyme complexes. The hydroxyl group is oriented away from residue 73 and the methyl group is in a pocket defined by Val120, Leu158 and Ala69<sup>36,38</sup>(Figs. 4A, 6A,B). The orientation of the hydroxyl group away from the pocket that would contain the carboxylated Lys73 general base and the deacylating water indicates it would not inactivate these groups as it is suggested to do in non-carbapenemase enzymes<sup>30,32</sup>. This finding is consistent with the relatively fast deacylation rate for imipenem (Table 1). A notable difference between our OXA-48 K73A/imipenem structure and previous structures is the conformation of Ser118 (Figs. 4A, 6A,B). In previous structures, the Ser118 rotamer has a χ<sub>1</sub>~-150° value while the K73A/imipenem structure has a Ser118 rotamer with χ<sub>1</sub>~-60° (Figs. 4A, 6A). This is likely due to the K73A substitution, which eliminates a hydrogen bond between Lys73 and Ser118 that stabilizes the χ<sub>1</sub>~-150° conformation.

The OXA-48 K73A/meropenem acyl-enzyme structure was determined at 1.84 Å resolution (Fig. 4C, Table 2). This structure is also very similar to previously determined OXA-48/meropenem acyl-enzyme structures with the meropenem carbonyl oxygen in the oxyanion hole, the C3 carboxylate making hydrogen bonds to Thr209 and Arg250, and the hydroxyethyl group oriented as in the OXA-48 K73A/imipenem structure with the methyl group in the hydrophobic pocket formed by Ala69, Val120, and Leu158 and the hydroxyl oriented away from Lys73 where it would not interfere with the general base or deacylation water (Figs. 4C, 5, 6C,D). While this orientation of the hydroxyethyl group is consistent with meropenem hydrolysis, it does not offer a ready explanation for why meropenem is deacylated at a slower rate than imipenem. As with the imipenem structure, the effect of the K73A mutation is a change in the rotamer distribution of Ser118. Finally, the weak density and high B-factors of the C2 substituent suggests the meropenem C2 substituent is flexible in the structure.

Figure 6

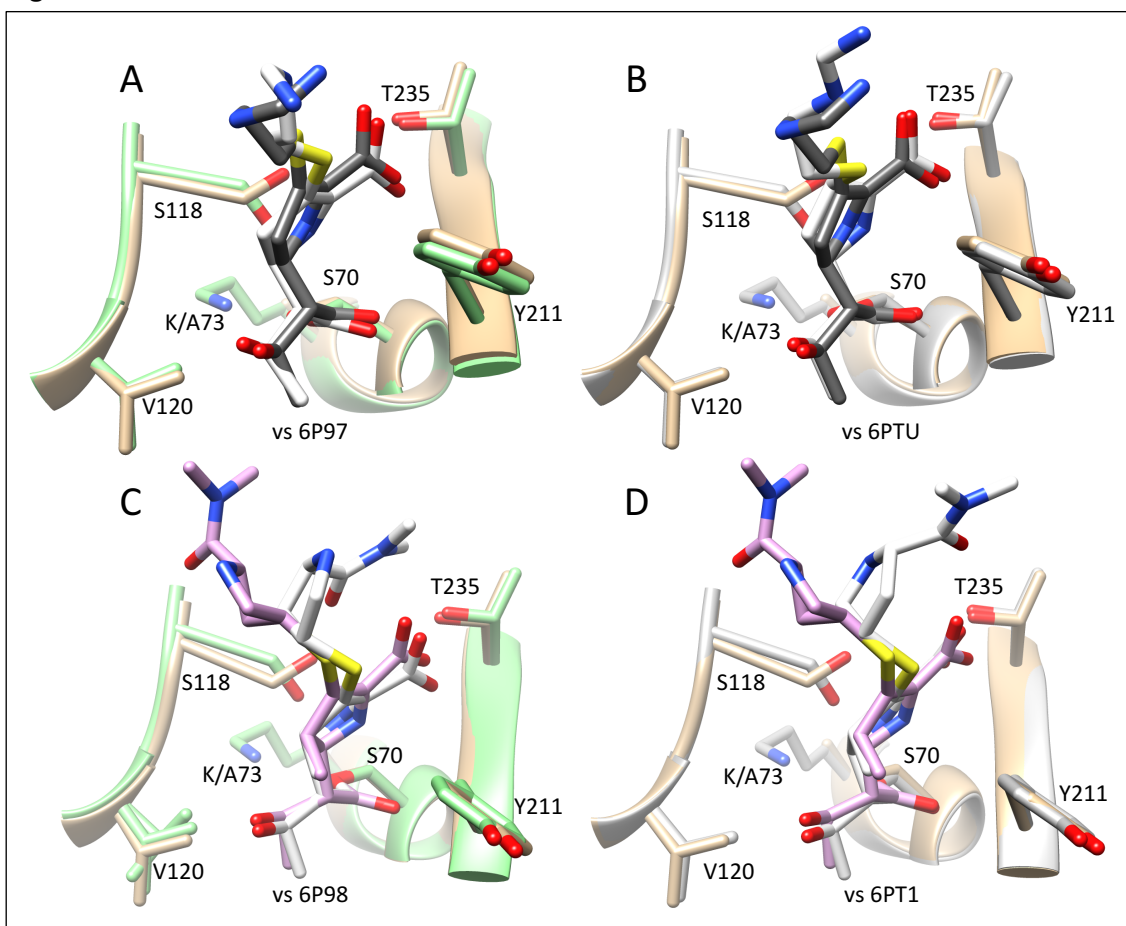


**Figure 6.** X-ray crystal structures of the OXA-48 K73A acyl-enzyme complexes with imipenem and meropenem superimposed with previously determined structures. **A.** OXA-48 K73A(tan)/imipenem(gray) aligned with OXA-48(green)/imipenem(white) (PDB id:6P97). **B.** OXA-48 K73A(tan)/imipenem(gray) aligned with OXA-48(white)/imipenem(white) (PDB id:6PTU). **C.** OXA-48 K73A(tan)/meropenem(pink) aligned with OXA-48(green)/meropenem(white) (PDB id:6P98). **D.** OXA-48 K73A(tan)/meropenem(pink) aligned with OXA-48(white)/meropenem(white) (PDB id:6PT1).

*X-ray structures of OXA-163 K73A mutant reveal multiple conformations of carbapenems in the active site*

As noted above, the OXA-163 enzyme contains the S212D substitution and 214-RIEP-217 deletion compared to OXA-48, which results in an increased rate of oxyiminocephalosporin hydrolysis but a drastically decreased rate of carbapenem hydrolysis due to slow deacylation<sup>27</sup>. To understand the basis for the decreased carbapenem hydrolysis rate, we determined the acyl-enzyme structures of an OXA-163 K73A mutant in complex with imipenem and meropenem. The OXA-163 K73/imipenem complex crystallized with one molecule in the asymmetric unit in the C222<sub>1</sub> space group and the structure was

determined at 1.88 Å resolution (Fig. 4B, Table 2). As with the OXA-48 K73A/imipenem structure, the imipenem carbonyl oxygen is in the oxyanion hole and the C3 carboxylate group makes hydrogen bonds to the side chains of Thr209 and Arg250 (Fig. 4A,B, 5). In addition, the C2 group is planar with the ring, indicating  $sp^2$  hybridization consistent with the  $\Delta^2$  tautomer. A further similarity is the presence of the Ser118  $\chi_1 \sim -60^\circ$  rotamer conformation, presumably due to the K73A substitution (Fig. 4B). Finally, the hydroxyethyl group is positioned as in the OXA-48 K73A/imipenem structure with the hydroxyl oriented away from Lys73 where it would not interfere with the general base or deacylation water.

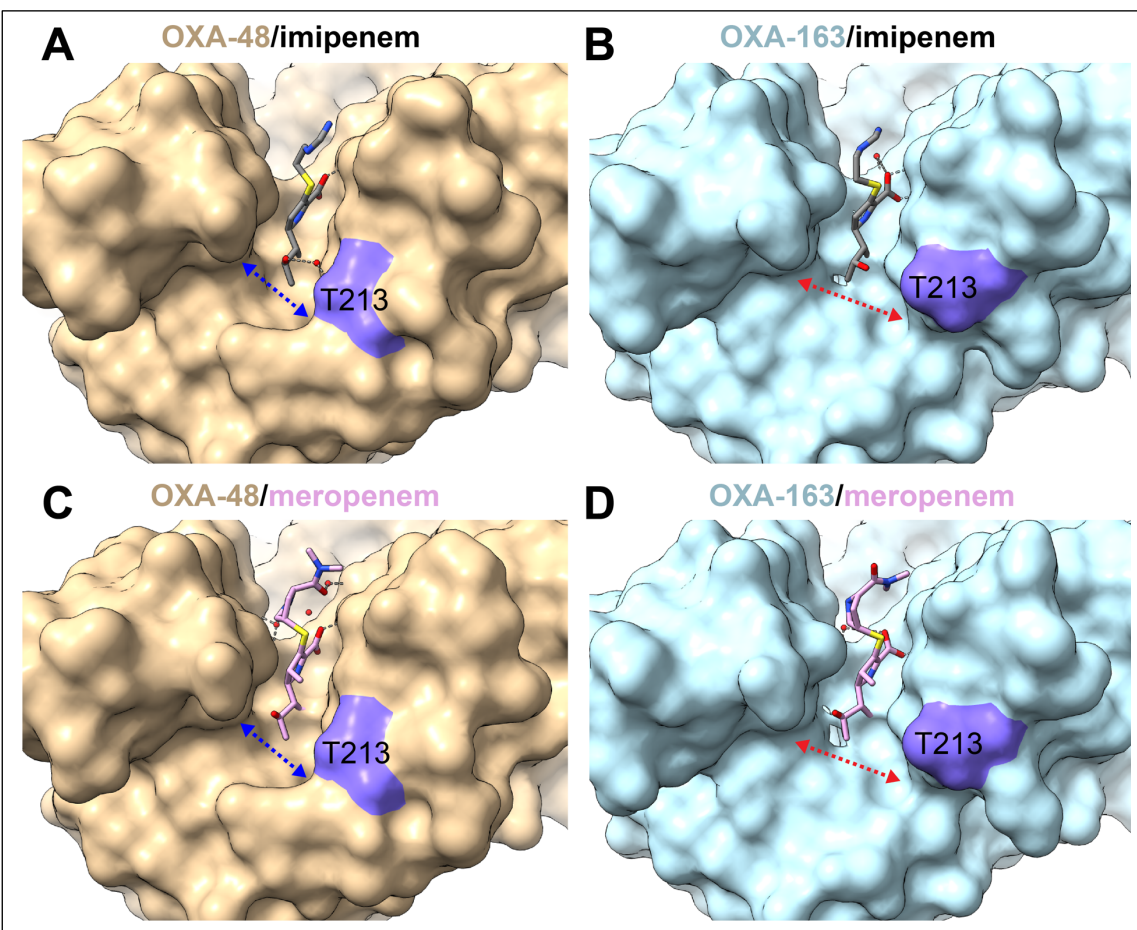


**Figure 7.** Surface representation of the OXA-48 and OXA-163 structures with imipenem and meropenem. **A.** OXA-48 structure with acylated imipenem showing the  $\beta_5$ - $\beta_6$  loop constraint of the active site size near the  $6\alpha$ -hydroxyethyl group. Imipenem carbons are shown in gray and the OXA-48 surface is shown in tan. The position of Thr213 is shown in purple. **B.** OXA-163 structure with acylated imipenem showing the reduced size of the  $\beta_5$ - $\beta_6$  loop due to the 214-RIEP-217 deletion that creates a wider active site near the  $6\alpha$ -hydroxyethyl group. The OXA-163 surface is shown in light blue. **C.** OXA-48 structure with acylated meropenem showing the constrained region near the  $6\alpha$ -hydroxyethyl group. Meropenem carbons are shown in pink. **D.** OXA-163 structure with acylated meropenem showing the wider active site in the region of the  $6\alpha$ -hydroxyethyl group.

There are also differences in the OXA-163 K73A/imipenem structure compared to the OXA-48 K73A/imipenem structure. The major difference is that the 214-RIEP-217 deletion creates a large opening in the active site that is absent in the OXA-48 K73A/imipenem structure (Fig. 4A,B, 7A,B). For example, Thr213 is displaced by 2.33 Å, which leads to the loss of interactions with the 6 $\alpha$ -hydroxyethyl group, suggesting that the larger active site might place fewer constraints on the conformation of the 6 $\alpha$ -hydroxyethyl group (Fig. 7B, Table 1).

The OXA-163 K73A meropenem-bound acyl-enzyme structure was determined at 1.88 Å resolution in the same space group and asymmetric unit specification as for the imipenem structure (Table 2). Meropenem is hydrolyzed by OXA-48 with a 20-fold lower  $k_{\text{cat}}$  than imipenem due to slower deacylation (Table 1). OXA-163, however, hydrolyzes meropenem with a  $k_{\text{cat}}$  a further 5-fold slower than OXA-48 due to even slower deacylation. As with the OXA-163/imipenem structure, the OXA-163 K73A/meropenem structure showed residual electron density extending from the O $\gamma$  of Ser70, indicative of covalently bound meropenem (Fig. 4D). Many of the polar and hydrophobic interactions of meropenem with the OXA-163 enzyme are identical with the imipenem interactions (Fig. 4B,D). Specifically, the formation of the oxyanion hole by the –NH of Ser70 and the –NH of Tyr211 and the coordination of the C3 carboxyl by Thr209 and Arg250 are similar (Fig. 5). The pyrroline ring of meropenem also demonstrated a planar-like appearance indicating  $sp^2$ -hybridization of the C2 carbon and the presence of the  $\Delta^2$ -tautomer. The R2 group of meropenem shows flexibility as indicated by weaker electron density and higher B-factors (Fig. 4D). Finally, as with the OXA-48 K73A/imipenem, OXA-48 K73A/meropenem and OXA-163 K73A/imipenem structures, the hydroxyethyl group is bound with the hydroxyl oriented away from Lys73 where it would not interfere with the general base or deacylation water.

The structural results suggest that the slow rate of deacylation of carbapenems by OXA-163 is not due to the hydroxyl oxygen of the 6 $\alpha$ -hydroxyethyl group hydrogen bonding to the carbamylated Lys73 or deacylating water to lower basicity or nucleophilicity, respectively. Alternatively, it is possible that the slow deacylation of both imipenem and meropenem by OXA-163 is due to a larger active site that does not adequately constrain the carbapenem acyl-enzyme leading to conformational heterogeneity (Fig. 7B,D). The existence of multiple, inactive conformations of the acyl-enzyme could account for the slow deacylation of both carbapenems.

#### *Molecular dynamics simulations reveal OXA-163 carbapenem complexes are unstable in the active site*

The basis for the different rates of acyl-enzyme hydrolysis between imipenem and meropenem for OXA-48 and OXA-163 was evaluated using molecular dynamics simulations. For this purpose, the structures of the imipenem and meropenem acyl-enzymes of the OXA-48 K73A and OXA-163 K73A mutants were used to construct models of the enzymes with Lys73 restored and carboxylated and with the substrate bound in the active site. The modified structures were subjected to energy minimization with steepest descent and ABNR minimization steps. Subsequently, the minimized simulation systems were subjected to 40 ps equilibrium MD simulations gradually raising the temperature

from 100K to 300K. The production MD simulations were carried out as NTP ensemble MD simulations at 300 K and 1 atm for 100 ns (Materials and Methods).

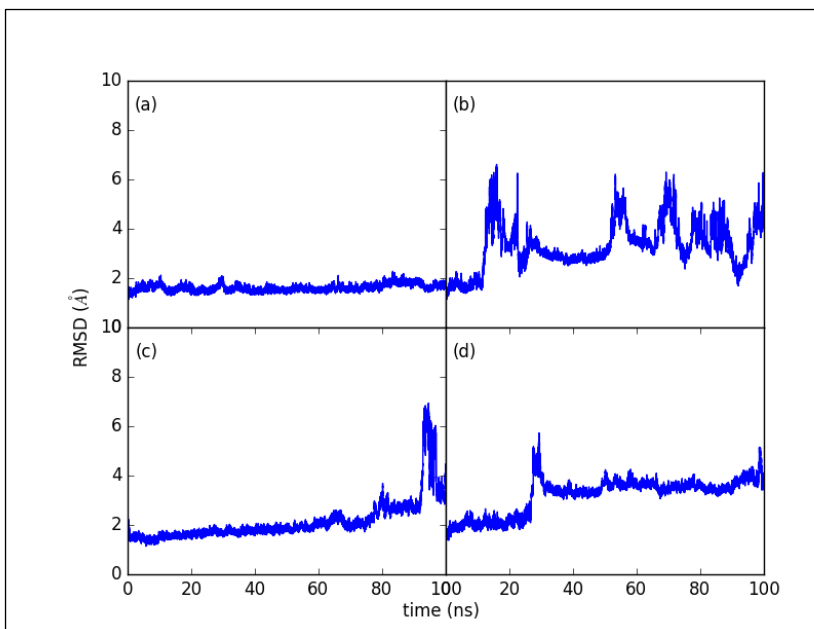


**Figure 8.** The RMSD of heavy atoms in the enzyme and substrate complex of four simulations. (a) OXA-48 with imipenem (b) OXA-163 with imipenem, (c) OXA-48 with meropenem, and (d) OXA-163 with meropenem.

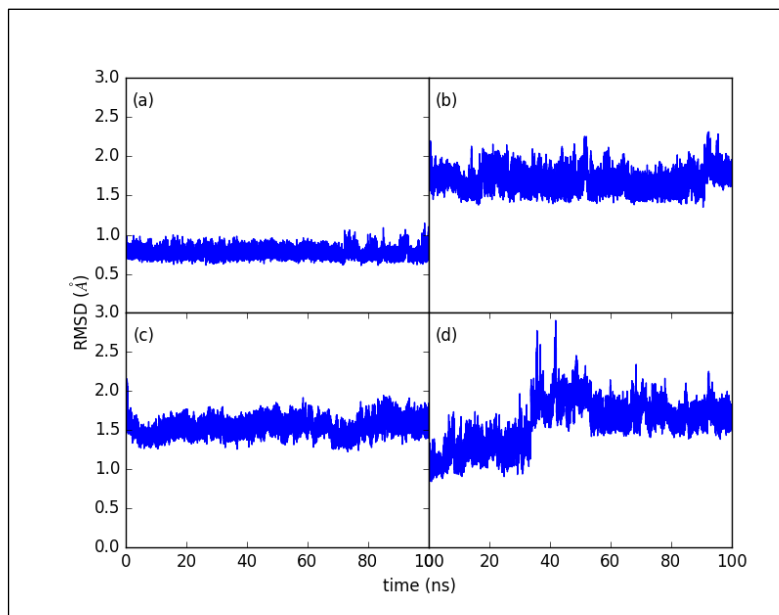


**Figure 9.** The RMSD of heavy atoms of active site amino acids of four simulations. (a) OXA-48 with imipenem (b) OXA-163 with imipenem, (c) OXA-48 with meropenem, and (d) OXA-163 with meropenem.

The root-mean-square deviation (RMSD) distribution of heavy atoms of the entire OXA-48 and OXA-163 enzymes plus substrate as well as the active site region plus substrate were calculated. For this purpose, residues including Ser70, Kcx73, Ser118, Trp157, and Lys208 were defined as the active site region due to their importance in substrate binding and the catalytic mechanism. The RMSD of OXA-48, non-covalently complexed with imipenem consistently fluctuates below 2 Å throughout the 100 ns MD simulation and the imipenem remains bound to the active site (Fig. 8A). The RMSD of OXA-48 complexed with meropenem is consistently lower than 2 Å during the first 60 ns of the simulation and increases during the remainder of the simulation (Fig. 8C). At 80 ns, it increases to ~4 Å and visual inspection reveals that meropenem leaves the active site. The RMSD of OXA-163 complexed with imipenem starts below 2 Å, but quickly increases at 10 ns and reaches above 6 Å (Fig. 8B). Overall, the RMSD has significant fluctuation ranging between 3 Å and 6 Å throughout the simulation for the OXA-163/imipenem complex. The imipenem ligand leaves the OXA-163 active site at approximately 10 ns but does rebind with the protein. The RMSD of the simulation of OXA-163 complexed with meropenem starts at ~2 Å, and has a sudden increase at around 25 ns and reaches above 5 Å (Fig. 8D). The ligand meropenem leaves the OXA-163 active site at 25 ns and stays close to but does not rebind with the protein.

To further investigate the dynamical behavior of OXA-48 and OXA-163 catalytic sites with ligands, the RMSD of heavy atoms of the active site amino acids for each simulation are plotted in Figure 9. The RMSD of OXA-48 complexed with imipenem consistently fluctuates around 1Å throughout the 100 ns MD simulations (Fig. 9A). The RMSD of OXA-48 complexed with meropenem fluctuates around 1.5 Å during the 100 ns MD simulations (Fig. 9C). The RMSD of the OXA-163 active site when complexed with imipenem fluctuates between 1.5Å and 2Å throughout the simulations (Fig. 9B). The RMSD of the OXA-163 active site when complexed with meropenem is the most flexible with the highest values and largest fluctuation throughout the simulation (Fig. 9D).

The above analyses suggest, first, that OXA-48 has a more stable binding mode with imipenem than with meropenem and meropenem (but not imipenem) actually leaves the active site during the simulation. This is consistent with the faster hydrolysis of imipenem compared to meropenem by OXA-48 (Table 1). In addition, OXA-48 exhibits more stable binding of both substrates than OXA-163. This is consistent with the finding that OXA-48 catalyzes the hydrolysis of the carbapenems faster than OXA-163 (Table 1). Thus, there is an inverse correlation between the extent of RMSD fluctuation and the rate of catalysis, i.e., a high degree of fluctuation corresponds to slow catalysis. Slow catalysis is, therefore, associated with the carbapenem substrate and associated active site residues sampling multiple conformations or sub-states. If the multiple conformations are largely non-productive the rate of hydrolysis would be slower<sup>49</sup>. A caveat is that the MD simulations were performed on the substrate complexes while the rate-determining step for the reactions is deacylation. The strong correlation between the extent of fluctuations observed (RMSD) and the rate of deacylation, however, suggests the stability of the non-covalent substrate complex is a reflection of the stability of the acyl-enzyme complex.

## Discussion

The OXA-48-like enzymes represent a group with high clinical importance<sup>19</sup>. OXA-48, the first and most widespread member of OXA-48-like enzymes, is a major contributor to carbapenem resistance among *Klebsiella pneumoniae* infections worldwide and is spreading at an alarming rate<sup>10</sup>. OXA-163 is a natural variant of OXA-48 with a different substrate profile wherein it gains hydrolytic activity against oxyimino-cephalosporins but loses activity towards carbapenems<sup>26,27</sup>. Here we present mechanistic and structural information on the interactions of OXA-48 and OXA-163 enzymes with the clinically important carbapenem  $\beta$ -lactam antibiotics, imipenem and meropenem. Our detailed kinetic studies show that deacylation is the rate-limiting step in the hydrolysis of carbapenems catalyzed by OXA-48 and OXA-163. Furthermore, the very slow hydrolysis of carbapenems by OXA-163 results largely from specific slowing of the deacylation rate compared to OXA-48. Substrate binding and acylation rates are comparable and cannot account for the activity changes. This mechanistic information in combination with the structures of the acyl-enzyme complexes of both enzymes with imipenem and meropenem provides insights into the hydrolysis of carbapenems by the OXA-48 and OXA-163 enzymes.

The OXA-48 enzyme shows higher turnover of both imipenem and meropenem than OXA-163 due to faster deacylation. Comparisons of the SFC-1 class A carbapenemase versus non-carbapenemase class A enzymes using structural and molecular dynamics data suggest the hydroxyl group of the  $6\alpha$ -hydroxyethyl side chain hydrogen bonds to the deacylation water in non-carbapenemases while in the SFC-1 carbapenemase the hydroxyl group is restrained away from the water<sup>32</sup>. However, the hydroxyl oxygen of the  $6\alpha$ -hydroxyethyl side chain is oriented away from the cavity containing the carbamylated Lys73 and deacylation water in both the OXA-48 and OXA-163 structures with imipenem and meropenem, suggesting this is not the mechanism for the slow reactions of OXA-163 (Fig. 4). An alternate hypothesis that is consistent with the structural results is that the deacylation rate is correlated with the conformational stability of the carbapenem acyl-enzyme intermediate. By this view, the OXA-48 imipenem and meropenem acyl-enzyme intermediates are more stable and sample fewer conformations than the OXA-163 acyl-enzymes. Further, we suggest a difference in stability of acylated imipenem and meropenem in the OXA-48 complexes could explain the faster deacylation of imipenem versus meropenem by this enzyme. If the increased stability also applies to the transition state, it would lead to the observed faster deacylation of imipenem by OXA-48 and the faster deacylation of both imipenem and meropenem by OXA-48 versus OXA-163. We further hypothesize that this effect is more prominent for the OXA-163 carbapenem acyl-enzyme intermediates where the S212D substitution and deletion in the  $\beta$ 5- $\beta$ 6 loop region creates a larger active site that does not adequately constrain the carbapenem acyl-enzyme. This results in the intermediate and the transition state assuming multiple conformations, most of which are inconsistent with rapid deacylation (Fig. 6).

Molecular dynamics simulations of the OXA-48 and OXA-163 enzymes in complex with imipenem and meropenem further support the idea that a failure to constrain the conformations of the acyl-enzyme reduces the deacylation rate. We found that OXA-48 has a more stable binding mode with imipenem than with meropenem, which is consistent with the faster hydrolysis of imipenem versus meropenem by OXA-48.

Furthermore, OXA-48 exhibits more stable binding of both imipenem and meropenem than OXA-163, which is consistent with the finding that OXA-48 catalyzes the hydrolysis of the carbapenems faster than OXA-163.

Previous structural and experimental studies of OXA-48 are also consistent with the hypothesis that the  $\beta$ 5- $\beta$ 6 loop region is important for the conformational stability of the carbapenem acyl-enzyme intermediate. Based on the structure of OXA-48 and molecular dynamics simulations of a modeled acyl-meropenem intermediate, the unique structure and conformation of the  $\beta$ 5- $\beta$ 6 loop region of OXA-48 is a key contributor to its carbapenemase activity<sup>22</sup>. It provides a binding site for the methyl-group of the 6 $\alpha$ -hydroxyethyl side chain that results in a conformation allowing access of water to the carbonyl carbon for deacylation<sup>22</sup>. An important role for the  $\beta$ 5- $\beta$ 6 loop is also supported by the gain in carbapenemase activity when the  $\beta$ 5- $\beta$ 6 loop from the carbapenemase, OXA-48 (and OXA-24) is grafted in place of the loop in the non-carbapenemase OXA-10<sup>50</sup>. It was further noted that the PXXG sequence motif found in the C-terminal section of the  $\beta$ 5- $\beta$ 6 loop is found in class D carbapenemases but not in other class D  $\beta$ -lactamases. Our data are consistent with these observations in that OXA-163, which contains a partial deletion of the  $\beta$ 5- $\beta$ 6 loop including the proline from the PXXG sequence, exhibits significantly lower  $k_{\text{cat}}$  values for carbapenem hydrolysis compared to OXA-48 that has an intact loop. Moreover, the results further indicate that the  $\beta$ 5- $\beta$ 6 loop is important for efficient deacylation of carbapenem acyl-enzyme intermediates since the lower  $k_{\text{cat}}$  values are due to slower deacylation.

Restraining the conformational stability of enzyme/substrate or enzyme/intermediate complexes has been suggested as an important aspect of catalytic efficiency and substrate specificity for several systems. For example, conformational stability has been proposed to explain negative epistasis between TEM-1  $\beta$ -lactamase mutations that extend the substrate specificity to oxyimino-cephalosporins<sup>49</sup>. In this system, individual substitutions increase enzyme conformations that increase active site access and enhance oxyimino-cephalosporin hydrolysis but combinations of mutations leads to disorder and sampling of many unproductive conformations<sup>49</sup>. In addition, directed evolution studies of the LovD enzyme that catalyzes an acyl transfer reaction showed that the trajectory of evolution towards a new substrate shows changes towards less conformational flexibility that results in enhanced catalytic activity<sup>51</sup>. The results of our mechanistic and structural study of OXA-48 and OXA-163 suggests restraining conformational flexibility of the carbapenem acyl-enzyme intermediate and the corresponding transition state is an important aspect of class D carbapenemase function.

**Table 2.** Crystal data collection and structure refinement statistics.

	OXA48 K73A/ imipenem	OXA48 K73A/ meropenem	OXA163 K73A/ imipenem	OXA163 K73A/ meropenem
<b>PDB ID</b>	<b>7KH9</b>	<b>7KHQ</b>	<b>7KHZ</b>	<b>7KHY</b>
<b>Data Collection</b>				
Wavelength (Å)	1.54	0.997	0.997	0.997
Resolution range (Å)	26.87 – 2.29 (2.37 – 2.29)	34.24 – 2.0 (2.04 – 2.0)	44.16 – 2.04 (2.11 – 2.04)	43.9 – 1.84 (1.94 – 1.84)
Space group	P 2 2 <sub>1</sub> 2 <sub>1</sub>	P 2 2 <sub>1</sub> 2 <sub>1</sub>	C 2 2 2 <sub>1</sub>	C 2 2 2 <sub>1</sub>
Unit cell				
<i>a, b, c</i> (Å)	44.7, 104.8, 125.1	44.3, 105.5, 125.7	44.4, 88.3, 125.4	44.3, 87.8, 125.0
$\alpha, \beta, \gamma$ (°)	90, 90, 90	90, 90, 90	90, 90, 90	90, 90, 90
Total reflections	53411 (5218)	334567 (15962)	31234 (3027)	42948 (4223)
Unique reflections	27105 (2650)	40232 (1925)	15808 (1538)	21551 (2118)
Multiplicity	2.0 (2.0)	8.3 (8.3)	2.0 (2.0)	6.7 (6.9)
Completeness (%)	99.4 (99.1)	99.1 (98.0)	98.0 (97.2)	99.6 (99.6)
Mean I/sigma(I)	10.73 (2.25)	11.02 (1.20)	11.63 (2.10)	15.88 (4.25)
Wilson B-factor	27.8	22.2	20.3	19.80
R-merge (%)	5.1 (25.2)	9.4 (66.6)	5.0 (26.0)	7.7 (39.4)
<b>Refinement</b>				
R <sub>work</sub> (%)/R <sub>free</sub> (%)	18.3/22.7	20.8/23.6	18.6/23.6	19.2/24.0
Total numbers of atoms	4318	4283	2098	2120
Protein residues	484	484	237	237
RMS (bonds)	0.003	0.005	0.003	0.004
RMS (angles)	0.768	0.615	0.645	0.684
Ramachandran analysis				
favored (%)	97.7	97.9	98.3	98.7
allowed (%)	2.3	2.1	1.7	1.3
outliers (%)	0	0	0	0
Average B-factor	28.1	29.0	24.5	23.4
protein	27.7	28.5	23.8	22.6
ligands	39.0	41.2	44.9	38.2
solvent	32.2	34.6	31.2	30.2

## Methods

### *Plasmids and site-directed mutagenesis*

The *bla*<sub>OXA-48</sub> and *bla*<sub>OXA-163</sub> protein expression plasmids were constructed by insertion of the  $\beta$ -lactamase genes into pET29a as has been described previously<sup>27</sup>. The K73A amino acid substitution was introduced into OXA-48 and OXA-163 by PCR

mutagenesis with PfuTurbo DNA Polymerase (Agilent Technologies Santa Clara, CA, USA) according to the manufacturer guidelines. DNA sequencing of the entire *bla* gene for each mutant was performed to ensure the absence of extraneous mutations.

#### *Protein Expression and Purification*

OXA-48 and OXA-163  $\beta$ -lactamases and their respective K73A mutants were expressed in *E. coli* BL21(DE3) cells and purified by affinity and size-exclusion chromatography. In brief, 1L LB broth containing 30  $\mu\text{g}/\text{mL}$  kanamycin was inoculated with 10 mL of overnight cell culture and incubated at 37°C until it reached an  $\text{OD}_{600}$  of 0.6-0.8 before induction with 0.5 mM IPTG. The culture was then grown at 25°C for 18-20 hours with shaking. Cell pellets were obtained by centrifugation at 7000 rpm for 30 minutes and resuspended in 30 mL of buffer containing 20 mM Tris-HCl pH 8.2 and 20% w/v sucrose. Addition of 60 mL of distilled water with vigorous shaking for 5 minutes was used to induce periplasmic content release. The resulting spheroblasts were pelleted by centrifugation and the supernatant was filtered using 0.22  $\mu\text{m}$  filters (Corning, NY, USA) before addition of 10 mL of 4M NaCl (400 mM final concentration). The filtrate was loaded onto a Fast Flow Chelating Sepharose™ packed column (GE Healthcare, Pittsburgh, PA) charged with zinc. The proteins were eluted with a linear gradient of 150 mM imidazole. The eluted fractions were checked by sodium dodecyl sulfate–polyacrylamide gel electrophoresis (SDS–PAGE). Fractions containing  $\beta$ -lactamases were concentrated using Amicon centrifugal filters 10,000 MW cut-off (Merck KGaA, Darmstadt, Germany). After concentration, size-exclusion chromatography using a HiLoad 16/600 Superdex 75 column (GE Healthcare) was performed in 25 mM Tris-HCl (pH 7.7), 25 mM NaCl and 5 mM  $\text{NaHCO}_3$ .  $\beta$ -lactamase fractions were concentrated and protein concentrations were determined by absorbance at 280 nm using an extinction coefficient of 63,940  $\text{M}^{-1} \text{cm}^{-1}$ .

#### *Steady-state kinetics*

Assays were performed on a DU800 spectrophotometer at room temperature (23°C) in 50 mM  $\text{NaP}_i$  buffer (pH 7.2) supplemented with 20 mM  $\text{NaHCO}_3$  as previously described<sup>27</sup>.  $\beta$ -Lactam hydrolysis was monitored at a wavelength of 298 nm for meropenem ( $\Delta\epsilon = -7200 \text{ M}^{-1} \text{cm}^{-1}$ ), and 299 nm for imipenem ( $\Delta\epsilon = -9670 \text{ M}^{-1} \text{cm}^{-1}$ ). Initial rates were plotted and fit to the Michaelis-Menten equation by non-linear regression with GraphPad Prism 6 software (GraphPad Software, Inc., La Jolla, CA).

#### *Acylation rates ( $k_2$ ) for carbapenem hydrolysis*

The linear pathway of  $\beta$ -lactam hydrolysis by serine  $\beta$ -lactamases is outlined in Scheme 1 and consists of two distinct chemical steps (acylation and deacylation) that are associated with the rate constants  $k_2$  (acylation) and  $k_3$  (deacylation) (Scheme 1).

The rate constant for acylation ( $k_2$ ) of carbapenems was determined by pre-steady-state kinetics under single turnover conditions using a KinTek Model SF-2001 stopped-flow apparatus (KinTek Corporation, Clearance, PA)<sup>45</sup>. The reactions were performed at 23°C. Reactions were performed in 50 mM  $\text{NaP}_i$  buffer (pH 7.2) supplemented with 20 mM  $\text{NaHCO}_3$ . The meropenem reaction was monitored at a wavelength of 298 nm ( $\Delta\epsilon = -7200 \text{ M}^{-1} \text{cm}^{-1}$ ), and the imipenem reaction was monitored

at 299 nm ( $\Delta\epsilon = -9670 \text{ M}^{-1} \text{ cm}^{-1}$ ). The substrate and enzyme were mixed in a 1:1 ratio by volume. 7.5  $\mu\text{M}$  of substrate was used with increasing concentrations of enzyme from 10-640  $\mu\text{M}$ . For each enzyme concentration, 10-15 measurements were made and averaged. The reaction was followed for 0.1 to 2 seconds and the curves were fit to a single exponential equation (Equation 1) to obtain  $k_{obs}$ . The resulting  $k_{obs}$  values were fitted with Equation 2 where  $K' = (k_{-1} + k_2)/k_1$ .

$$A_t = A_0 e^{-k_{obs}t} + C \quad \text{Equation 1}$$

$$k_{obs} = \frac{k_2[S]}{(K' + [S])} \quad \text{Equation 2}$$

### Deacylation rates ( $k_3$ ) for carbapenem hydrolysis

Deacylation rates were determined by the reactivation method<sup>46</sup>. Enzymes were incubated with carbapenems at a concentration of at least 10-fold the  $K_m$  value for 0.1-30 minutes in 50 mM NaP<sub>i</sub> buffer (pH 7.2) supplemented with 20 mM NaHCO<sub>3</sub>. Various incubation times were tested to assure full recovery of the activity. After the incubation, the mixtures were diluted 100-200-fold in buffer containing nitrocefin, which was used as a reporter substrate. The final concentration of enzymes was 20 nM for OXA-48 and 30 nM for OXA-163. The final concentration of nitrocefin was 350  $\mu\text{M}$ , which is 10-fold higher than the  $K_m$  for both enzymes. Reactions without carbapenem incubation were also performed as a control. The reactivation reaction was monitored by nitrocefin hydrolysis at 482 nm ( $\Delta\epsilon = 20,500 \text{ M}^{-1} \text{ cm}^{-1}$ ). The deacylation rate constants ( $k_3$ ) were determined by fitting the progress curves with Equation 3 where  $v_s$  is the velocity of nitrocefin hydrolysis at time  $t$ . It was not possible to measure the  $k_3$  value of OXA-48 for imipenem hydrolysis because of the high  $k_{cat}$  value. Instead, Equation 4 was used to derive  $k_3$  for OXA-48 with imipenem using the experimentally determined values for  $k_2$  and  $k_{cat}$ . Solving Equation 4 for  $k_{cat}$  in terms of  $k_3$  gives  $k_3 = (k_2 * k_{cat}) / (k_{cat} - k_2)$ . The error on the calculated  $k_3$  value was determined by propagating the error on  $k_{cat}$  and  $k_2$  through the equation by adding the absolute errors for the sum(difference) in the denominator to obtain the absolute and the percentage error in  $k_{cat} - k_2$ . The percent error of the numerator, ( $k_{cat} * k_2$ ), was calculated by adding the percent error for  $k_{cat}$  and  $k_2$  and the final, percent and absolute errors on  $k_3$  were then obtained by adding the percent error of the numerator and denominator to give the percentage error in  $k_3$ .

$$A_t = A_0 + v_s t - \frac{v_s}{k_3} (1 - e^{-k_3 t}) \quad \text{Equation 3}$$

$$k_{cat} = \frac{k_2 k_3}{k_2 + k_3} \quad \text{Equation 4}$$

### Protein crystallization and data collection

The hanging drop vapor diffusion method was used with a final protein concentration of 5-7 mg/mL in the drop. Crystallization conditions were screened with commercially available screens from Hampton Research (Aliso Viejo, CA) and Qiagen (Venlo, Netherlands) using a 96-well format. Initial crystallization conditions were optimized manually by setting up 24-well plates with 5  $\mu$ L final volume of the drops (1:1 protein-well solution). Protein-carbapenem co-crystals were produced in the following conditions: 100 mM Tris-HCl pH 8.5, 15% PEG 20000 for OXA-48 K73A with imipenem; 220 mM NaCOOH, 3% v/v 2-Methyl-2,4-pentanediol, and 24% PEG 3350 for OXA-163 K73A with imipenem; 200 mM lithium acetate dihydrate and 20% w/w PEG 3350 for OXA-48 K73A with meropenem and 240 mM NaCOOH, 3% v/v dimethyl sulfoxide, 22% PEG 3350 for OXA-163 K73A with meropenem. Data sets were collected at beamline 5.0.1 of the Berkeley Center for Structural Biology in the context of the Collaborative Crystallography Program except for the OXA-48 with imipenem data set, which was collected on the home source at Baylor College of Medicine with a Rigaku FR-E SuperBright High-Brilliance Rotating Anode Generator.

#### *Crystallography data processing and refinement*

Diffraction data were processed using the CCP4 suite<sup>52</sup>. Data were processed using iMOSFLM<sup>53</sup> and scaled and merged with AIMLESS<sup>54</sup>. Structures were determined by molecular replacement with MOLREP<sup>55</sup> using the wild-type structures as search models (OXA-48 PDB ID 3HBR and OXA-163 PDB ID 4S2L). The initial models were refined using REFMAC5<sup>56</sup> and/or PHENIX<sup>57</sup> as implemented in phenix.refine<sup>58</sup>. Manual inspection of the models was done throughout the refinement process using the Crystallography Object-Oriented Toolkit (COOT) program<sup>59,60</sup>. When appropriate, TLS groups were determined using the TLSMD server<sup>61</sup>. The structures were inspected with the PDB\_REDO server<sup>62</sup> and final refinement was done using either REFMAC5 or phenix.refine. The final structure was inspected and validated with MolProbity<sup>63</sup> and COOT<sup>60</sup>.

#### *Programs used and structure coordinates deposition*

Structural figures were generated using the UCSF Chimera graphical program<sup>64</sup>. The SSM procedure was used for superimposition of the structures as implemented in COOT<sup>60</sup>. The atomic coordinates of the structures were deposited in the Protein Data Bank with accession codes 7KH9, 7KHQ, 7KHZ, and 7KHY.

#### *Molecular dynamics simulations*

The crystal structures of OXA-48 and OXA-163 K73A mutants with carbapenem substrates (imipenem and meropenem) and bicarbonate (BCT) were subjected to molecular dynamics (MD) simulations using a molecular mechanics program suite, CHARMM program version 40b1<sup>65</sup> and CHARMM36 force field<sup>66</sup>thos. All systems were solvated in a water box using a TIP3P model<sup>67</sup> with the addition of sodium and chloride ions to balance the charge. The simulation boxes were subjected to 200 steps of the steepest descent energy minimization and further energy minimization using the adopted basis Newton-Raphson (ABNR) method until the total gradient of the system was lower than 0.03 kcal/mol $\cdot$ Å. Subsequently, the minimized simulation systems were subjected

to 12 picoseconds (ps) equilibrium gradually raising the temperature from 100K to 300K. The system was then equilibrated via 5 nanoseconds (ns) isothermal-isobaric (NTP) ensemble MD simulations at 300 K and 1 atm.

The last frame of the MD simulations was selected and residue 73 and BCT were modified into lysine Nz-carboxylic acid (Kcx) using CHARMM version 40b1.<sup>1</sup> The modified structures were subjected to energy minimization with steepest descent and ABNR minimization steps. Subsequently, the minimized simulation systems were subjected to 40 ps equilibrium MD simulations gradually raising the temperature from 100K to 300K. The system was then subjected to 100ns NTP ensemble MD simulations at 300 K and 1 atm as production simulations. In all MD simulations, the time step was 2 femtoseconds (fs), with all the bonds associated with hydrogen being fixed during the simulation. Periodic boundary conditions were applied in all simulations. Electrostatic interactions were modeled using the particle mesh Ewald method<sup>66,68</sup>.

Root-mean-square deviation (RMSD) was used to measure the difference of conformation for each snapshot of the MD simulations with regard to the reference structure. For a molecular structure represented by the Cartesian coordinate vector of  $N$  atoms, the RMSD is calculated as the following:

$$\text{RMSD} = \sqrt{\frac{\sum_{i=1}^N (r_i^0 - Ur_i)^2}{N}} \quad (\text{eq.1})$$

where  $r_i^0$  is the Cartesian coordinate vector for the optimized structure as reference and  $U$  is the best-fit alignment transformation matrix between a given structure and the reference structure. The RMSD indicates the conformational changes comparing with the reference structure. In the system, the residues Kcx73, Ser70, Ser118, Trp157, Lys208 amino acids were defined as the active site region. The conformational changes of the active site region can influence substrate binding and catalytic mechanism. Therefore, the RMSD of the heavy atoms of active site region and the RMSD of the heavy atoms of the whole protein plus substrate were calculated.

## Acknowledgments

This work was supported by NIH grant R01 AI32956 to TP, Welch Foundation Q1279 to BVVP, and NSF CAREER grant 1753167 to PT. The ALS-ENABLE beamlines are supported in part by the National Institutes of Health, National Institute of General Medical Sciences, grant P30 GM124169-01. The Advanced Light Source is a Department of Energy Office of Science User Facility under Contract No. DE-AC02-05CH11231. Computational time was provided by the Southern Methodist University's Center for Research Computing. The authors thank Dr. Hiram Gilbert for comments on the manuscript.

## References

- (1) Martens, E., and Demain, A. L. (2017) The antibiotic resistance crisis, with a focus on the United States. *J. Antibiot.* 70, 520–526.

- (2) Holmes, A. H., Moore, L. S. P., Sundsfjord, A., Steinbakk, M., Regmi, S., Karkey, A., Guerin, P. J., and Piddock, L. J. V. (2016) Understanding the mechanisms and drivers of antimicrobial resistance. *Lancet* 387, 176–187.
- (3) Nordmann, P., Cuzon, G., and Naas, T. (2009) The real threat of *Klebsiella pneumoniae* carbapenemase-producing bacteria. *Lancet Infect. Dis.* 9, 228–236.
- (4) Nordmann, P., Dortet, L., and Poirel, L. (2012) Carbapenem resistance in Enterobacteriaceae: here is the storm. *Trends Mol. Med.* 18, 263–272.
- (5) Guh, A. Y., Bulens, S. N., Mu, Y., Jacob, J. T., Reno, J., Scott, J., Wilson, L. E., Vaeth, E., Lynfield, R., Shaw, K. M., Vagnone, P. M. S., Bamberg, W. M., Janelle, S. J., Dumyati, G., Concannon, C., Beldavs, Z., Cunningham, M., Cassidy, P. M., Phipps, E. C., Kenslow, N., Travis, T., Lonsway, D., Rasheed, J. K., Limbago, B. M., and Kallen, A. J. (2015) Epidemiology of Carbapenem-Resistant Enterobacteriaceae in 7 US Communities, 2012–2013. *JAMA* 314, 1479–1487.
- (6) Poirel, L., Pitout, J. D., and Nordmann, P. (2007) Carbapenemases: molecular diversity and clinical consequences. *Future Microbiol.* 2, 501–512.
- (7) Paterson, D. L. (2006) Resistance in gram-negative bacteria: Enterobacteriaceae. *Am. J. Infect. Control* 34, S20–28; discussion S64–73.
- (8) Garbati, M. A., and Al Godhair, A. I. (2013) The growing resistance of *Klebsiella pneumoniae*; the need to expand our antibiogram: case report and review of the literature. *Afr. J. Infect. Dis.* 7, 8–10.
- (9) Broberg, C. A., Palacios, M., and Miller, V. L. (2014) *Klebsiella*: a long way to go towards understanding this enigmatic jet-setter. *F1000Prime Rep.* 6, 64.
- (10) Pitout, J. D. D., Nordmann, P., and Poirel, L. (2015) Carbapenemase-Producing *Klebsiella pneumoniae*, a Key Pathogen Set for Global Nosocomial Dominance. *Antimicrob. Agents Chemother.* 59, 5873–5884.
- (11) Nicolau, D. P. (2008) Carbapenems: a potent class of antibiotics. *Expert Opin. Pharmacother.* 9, 23–37.
- (12) Papp-Wallace, K. M., Endimiani, A., Taracila, M. A., and Bonomo, R. A. (2011) Carbapenems: past, present, and future. *Antimicrob. Agents Chemother.* 55, 4943–4960.
- (13) McKenna, M. (2013) Antibiotic resistance: the last resort. *Nature* 499, 394–396.
- (14) Rapp, R. P., and Urban, C. (2012) *Klebsiella pneumoniae* carbapenemases in Enterobacteriaceae: history, evolution, and microbiology concerns. *Pharmacotherapy* 32, 399–407.
- (15) Tang, S. S., Apisarnthanarak, A., and Hsu, L. Y. (2014) Mechanisms of  $\beta$ -lactam antimicrobial resistance and epidemiology of major community- and healthcare-associated multidrug-resistant bacteria. *Adv. Drug Deliv. Rev.* 78, 3–13.
- (16) Bush, K., and Jacoby, G. A. (2010) Updated functional classification of beta-lactamases. *Antimicrob. Agents Chemother.* 54, 969–976.
- (17) Ambler, R. P. (1980) The structure of beta-lactamases. *Phil. Trans. Ry. Soc. London, Ser. B* 289, 321–331.
- (18) Nordmann, P., Naas, T., and Poirel, L. (2011) Global spread of Carbapenemase-producing Enterobacteriaceae. *Emerging Infect. Dis.* 17, 1791–1798.
- (19) Poirel, L., Potron, A., and Nordmann, P. (2012) OXA-48-like carbapenemases, the phantom menace. *J. Antimicrob. Chemother.* 67, 1597–1606.

- (20) Nordmann, P., Poirel, L., Walsh, T. R., and Livermore, D. M. (2011) The emerging NDM carbapenemases. *Trends Microbiol.* *19*, 588–595.
- (21) Poirel, L., Héritier, C., Tolün, V., and Nordmann, P. (2004) Emergence of oxacillinase-mediated resistance to imipenem in *Klebsiella pneumoniae*. *Antimicrob. Agents Chemother.* *48*, 15–22.
- (22) Docquier, J.-D., Calderone, V., De Luca, F., Benvenuti, M., Giuliani, F., Bellucci, L., Tafi, A., Nordmann, P., Botta, M., Rossolini, G. M., and Mangani, S. (2009) Crystal structure of the OXA-48 beta-lactamase reveals mechanistic diversity among class D carbapenemases. *Chem. Biol.* *16*, 540–547.
- (23) Dortet, L., Oueslati, S., Jeannot, K., Tandé, D., Naas, T., and Nordmann, P. (2015) Genetic and biochemical characterization of OXA-405, an OXA-48-type extended-spectrum  $\beta$ -lactamase without significant carbapenemase activity. *Antimicrob. Agents Chemother.* *59*, 3823–3828.
- (24) Oueslati, S., Nordmann, P., and Poirel, L. (2015) Heterogeneous hydrolytic features for OXA-48-like  $\beta$ -lactamases. *J. Antimicrob. Chemother.* *70*, 1059–1063.
- (25) Gomez, S., Pasteran, F., Faccione, D., Bettiol, M., Veliz, O., De Belder, D., Rapoport, M., Gatti, B., Petroni, A., and Corso, A. (2013) Inpatient emergence of OXA-247: a novel carbapenemase found in a patient previously infected with OXA-163-producing *Klebsiella pneumoniae*. *Clin. Microbiol. Infect.* *19*, E233-235.
- (26) Poirel, L., Castanheira, M., Carrère, A., Rodriguez, C. P., Jones, R. N., Smayevsky, J., and Nordmann, P. (2011) OXA-163, an OXA-48-related class D  $\beta$ -lactamase with extended activity toward expanded-spectrum cephalosporins. *Antimicrob. Agents Chemother.* *55*, 2546–51.
- (27) Stojanoski, V., Chow, D.-C., Fryszczyn, B., Hu, L., Nordmann, P., Poirel, L., Sankaran, B., Prasad, B. V. V., and Palzkill, T. (2015) Structural Basis for Different Substrate Profiles of Two Closely Related Class D  $\beta$ -Lactamases and Their Inhibition by Halogens. *Biochemistry* *54*, 3370–3380.
- (28) Golemi, D., Maveyraud, L., Vakulenko, S., Tranier, S., Ishiwata, A., Kotra, L. P., Samama, J.-P., and Mobashery, S. (2000) The first structural and mechanistic insights for class D  $\beta$ -lactamases: Evidence for a novel catalytic process for turnover of  $\beta$ -lactam antibiotics. *J. Am. Chem. Soc.* *122*, 6132–6133.
- (29) Golemi, D., Maveyraud, L., Vakulenko, S., Samama, J. P., and Mobashery, S. (2001) Critical involvement of a carbamylated lysine in catalytic function of class D beta-lactamases. *Proc. Natl. Acad. Sci. U.S.A.* *98*, 14280–14285.
- (30) Maveyraud, L., Mourey, L., Kotra, L. P., Pedelacq, J.-D., Guillet, V., Mobashery, S., and Samama, J.-P. (1998) Structural Basis for Clinical Longevity of Carbapenem Antibiotics in the Face of Challenge by the Common Class A  $\beta$ -Lactamases from the Antibiotic-Resistant Bacteria. *J. Am. Chem. Soc.* *120*, 9748–9752.
- (31) Nukaga, M., Bethel, C. R., Thomson, J. M., Hujer, A. M., Distler, A., Anderson, V. E., Knox, J. R., and Bonomo, R. A. (2008) Inhibition of class A  $\beta$ -lactamases by carbapenems: Crystallographic observation of two conformations of meropenem in SHV-1. *J. Amer. Chem. Soc.* *130*, 12656–12662.
- (32) Fonseca, F., Chudyk, E. I., van der Kamp, M. W., Correia, A., Mulholland, A. J., and Spencer, J. (2012) The basis for carbapenem hydrolysis by class A  $\beta$ -lactamases: A combined investigation using crystallography and simulations. *J. Amer. Chem. Soc.* *134*, 18275–18285.

- (33) Tremblay, L. W., Fan, F., and Blanchard, J. S. (2010) Biochemical and structural characterization of *Mycobacterium tuberculosis*  $\beta$ -lactamase with the carbapenems ertapenem and doripenem. *Biochemistry* 49, 3766–3773.
- (34) Kalp, M., and Carey, P. R. (2008) Carbapenems and SHV-1 beta-lactamase form different acyl-enzyme populations in crystals and solution. *Biochemistry* 47, 11830–11837.
- (35) Toth, M., Smith, C. A., Antunes, N. T., Stewart, N. K., Maltz, L., and Vakulenko, S. B. (2017) The role of conserved surface hydrophobic residues in the carbapenemase activity of the class D  $\beta$ -lactamases. *Acta Crystallogr. D Struct. Biol.* 73, 692–701.
- (36) Akhtar, A., Pemberton, O. A., and Chen, Y. (2020) Structural Basis for Substrate Specificity and Carbapenemase Activity of OXA-48 Class D  $\beta$ -Lactamase. *ACS Infect. Dis.* 6, 261–271.
- (37) Akhter, S., Lund, B. A., Ismael, A., Langer, M., Isaksson, J., Christopeit, T., Leiros, H.-K. S., and Bayer, A. (2018) A focused fragment library targeting the antibiotic resistance enzyme - Oxacillinase-48: Synthesis, structural evaluation and inhibitor design. *Eur. J. Med. Chem.* 145, 634–648.
- (38) Smith, C. A., Stewart, N. K., Toth, M., and Vakulenko, S. B. (2019) Structural Insights into the Mechanism of Carbapenemase Activity of the OXA-48  $\beta$ -Lactamase. *Antimicrob. Agents Chemother.* 63.
- (39) Héritier, C., Poirel, L., Aubert, D., and Nordmann, P. (2003) Genetic and functional analysis of the chromosome-encoded carbapenem-hydrolyzing oxacillinase OXA-40 of *Acinetobacter baumannii*. *Antimicrob. Agents Chemother.* 47, 268–273.
- (40) Walther-Rasmussen, J., and Høiby, N. OXA-type carbapenemases. *J. Antimicrob. Chemother.* 57, 373–383.
- (41) Galleni, M., and Frere, J.-M. (2007) Kinetics of  $\beta$ -lactamases and penicillin-binding proteins., in *Enzyme-Mediated Resistance to Antibiotics: Mechanisms, Dissemination, and Prospects for Inhibition.* (Bonomo, R. A., and Tolmasky, M. E., Eds.), pp 67–79. ASM Press, Washington, D.C.
- (42) Palzkill, T. (2018) Structural and mechanistic basis for extended-spectrum drug-resistance mutations in altering the specificity of TEM, CTX-M, and KPC  $\beta$ -lactamases. *Front. Mol. Biosci.* 5, 16.
- (43) Frase, H., Shi, Q., Testero, S. A., Mobashery, S., and Vakulenko, S. B. Mechanistic basis for the emergence of catalytic competence against carbapenem antibiotics by the GES family of beta-lactamases. *J. Biol. Chem.* 284, 29509–29513.
- (44) Christensen, H., Martin, M., and Waley, G. (1990)  $\beta$ -Lactamases as fully efficient enzymes. *Biochem. J.* 266, 853–861.
- (45) Bicknell, R., and Waley, S. G. (1985) Single-turnover and steady-state kinetics of hydrolysis of cephalosporins by beta-lactamase I from *Bacillus cereus*. *Biochem. J.* 231, 83–88.
- (46) Koerber, S. C., and Fink, A. L. (1987) The analysis of enzyme progress curves by numerical differentiation, including competitive product inhibition and enzyme reactivation. *Anal. Biochem.* 165, 75–87.
- (47) Hollaway, M. R., Antonini, E., and Brunori, M. (1969) The ficin-catalysed hydrolysis of p-nitrophenyl hippurate. Detailed kinetics including the measurement

of the apparent dissociation constant for the enzyme-substrate complex. *FEBS Lett.* *4*, 299–306.

(48) June, C. M., Vallier, B. C., Bonomo, R. A., Leonard, D. A., and Powers, R. A. (2014) Structural origins of oxacillinase specificity in class D  $\beta$ -lactamases. *Antimicrob. Agents Chemother.* *58*, 333–341.

(49) Dellus-Gur, E., Elias, M., Caselli, E., Prati, F., Salverda, M. L., de Visser, J. A., Fraser, J. S., and Tawfik, D. S. (2015) Negative epistasis and evolvability in TEM-1  $\beta$ -lactamase—The thin line between an enzyme's conformational freedom and disorder. *J. Mol. Biol.* *427*, 2396–2409.

(50) De Luca, F., Benvenuti, M., Carboni, F., Pozzi, C., Rossolini, G. M., Mangani, S., and Docquier, J.-D. (2011) Evolution to carbapenem-hydrolyzing activity in noncarbapenemase class D  $\beta$ -lactamase OXA-10 by rational protein design. *Proc. Natl. Acad. Sci. U.S.A.* *108*, 18424–18429.

(51) Jiménez-Osés, G., Osuna, S., Gao, X., Sawaya, M. R., Gilson, L., Collier, S. J., Huisman, G. W., Yeates, T. O., Tang, Y., and Houk, K. N. (2014) The role of distant mutations and allosteric regulation on LovD active site dynamics. *Nat. Chem. Biol.* *10*, 431–436.

(52) Winn, M. D., Ballard, C. C., Cowtan, K. D., Dodson, E. J., Emsley, P., Evans, P. R., Keegan, R. M., Krissinel, E. B., Leslie, A. G., McCoy, A., McNicholas, S. J., Murshudov, G. N., Pannu, N. S., Potterton, E. A., Powell, H. R., Read, R. J., Vagin, A., and Wilson, K. S. (2011) Overview of the CCP4 suite and current developments. *Acta Crystallogr. D Biol. Crystallogr.* *67*, 235–42.

(53) Batty, T. G., Kontogiannis, L., Johnson, O., Powell, H. R., and Leslie, A. G. (2011) iMOSFLM: a new graphical interface for diffraction-image processing with MOSFLM. *Acta Crystallogr. D Biol. Crystallogr.* *67*, 271–281.

(54) Evans, P. R., and Murshudov, G. N. (2013) How good are my data and what is the resolution? *Acta Crystallogr. D Biol. Crystallogr.* *69*, 1204–1214.

(55) Vagin, A., and Teplyakov, A. (2010) Molecular replacement with MOLREP. *Acta Crystallogr. D Biol. Crystallogr.* *66*, 22–25.

(56) Vagin, A. A., Steiner, R. A., Lebedev, A. A., Potterton, L., McNicholas, S., Long, F., and Murshudov, G. N. (2004) REFMAC5 dictionary: organization of prior chemical knowledge and guidelines for its use. *Acta Crystallogr. D Biol. Crystallogr.* *60*, 2184–2195.

(57) Adams, P. D., Afonine, P. V., Bunkoczi, G., Chen, V. B., Davis, I. W., Echols, N., Headd, J. J., Hung, L. W., Kapral, G. J., Grosse-Kunstleve, R. W., McCoy, A. J., Moriarty, N. W., Oeffner, R., Read, R. J., Richardson, D. C., Richardson, J. S., Terwilliger, T. C., and Zwart, P. H. (2010) PHENIX: a comprehensive Python-based system for macromolecular structure solution. *Acta Crystallogr. D Biol. Crystallogr.* *66*, 213–21.

(58) Liebschner, D., Afonine, P. V., Baker, M. L., Bunkóczi, G., Chen, V. B., Croll, T. I., Hintze, B., Hung, L. W., Jain, S., McCoy, A. J., Moriarty, N. W., Oeffner, R. D., Poon, B. K., Prisant, M. G., Read, R. J., Richardson, J. S., Richardson, D. C., Sammito, M. D., Sobolev, O. V., Stockwell, D. H., Terwilliger, T. C., Urzhumtsev, A. G., Videau, L. L., Williams, C. J., and Adams, P. D. (2019) Macromolecular structure determination using X-rays, neutrons and electrons: recent developments in Phenix. *Acta Crystallogr. D Biol. Crystallogr.* *75*, 861–877.

(59) Emsley, P., and Cowtan, K. (2004) Coot: model-building tools for molecular graphics. *Acta Crystallogr. Biol. Crystallogr.* *60*, 2126–2132.

- (60) Emsley, P., Lohkamp, B., Scott, W. G., and Cowtan, K. (2010) Features and development of Coot. *Acta Crystallogr. D. Biol. Crystallogr.* 66, 486–501.
- (61) Painter, J., and Merritt, E. A. (2006) Optimal description of a protein structure in terms of multiple groups undergoing TLS motion. *Acta Crystallogr. D Biol. Crystallogr.* 62, 439–450.
- (62) Joosten, R. P., Long, F., Murshudov, G. N., and Perrakis, A. (2014) The PDB\_REDO server for macromolecular structure model optimization. *IUCrJ* 1, 213–220.
- (63) Chen, V. B., Arendall, W. B., Headd, J. J., Keedy, D. A., Immormino, R. M., Kapral, G. J., Murray, L. W., Richardson, J. S., and Richardson, D. C. (2010) MolProbity: all-atom structure validation for macromolecular crystallography. *Acta Crystallogr. D Biol. Crystallogr.* 66, 12–21.
- (64) Pettersen, E. F., Goddard, T. D., Huang, C. C., Couch, G. S., Greenblatt, D. M., Meng, E. C., and Ferrin, T. E. (2004) UCSF Chimera--a visualization system for exploratory research and analysis. *J. Comput. Chem.* 25, 1605–1612.
- (65) Halgren, T. The representation of van der Waals (vdW) interactions in molecular mechanics force fields: potential form, combination rules, and vdW parameters. *J. Am. Chem. Soc.* 114, 7827–7843.
- (66) Best, R. B., Zhu, X., Shim, J., Lopes, P. E. M., Mittal, J., Feig, M., and Mackerell, A. D. (2012) Optimization of the additive CHARMM all-atom protein force field targeting improved sampling of the backbone  $\phi$ ,  $\psi$  and side-chain  $\chi(1)$  and  $\chi(2)$  dihedral angles. *J. Chem. Theory Comput.* 8, 3257–3273.
- (67) Jorgensen, W. L., Chandrasekhar, J., Madura, J. D., Impey, R. W., and Klein, M. L. (1983) Comparison of simple potential functions for simulating liquid water. *J. Chem. Phys.* 79, 926–935.
- (68) Brooks, B. R., Brooks, C. L., Mackerell, A. D., Nilsson, L., Petrella, R. J., Roux, B., Won, Y., Archontis, G., Bartels, C., Boresch, S., Caflisch, A., Caves, L., Cui, Q., Dinner, A. R., Feig, M., Fischer, S., Gao, J., Hodoscek, M., Im, W., Kuczera, K., Lazaridis, T., Ma, J., Ovchinnikov, V., Paci, E., Pastor, R. W., Post, C. B., Pu, J. Z., Schaefer, M., Tidor, B., Venable, R. M., Woodcock, H. L., Wu, X., Yang, W., York, D. M., and Karplus, M. (2009) CHARMM: the biomolecular simulation program. *J. Comput. Chem.* 30, 1545–1614.

For Table of Contents Use Only

## Mechanistic Basis of OXA-48-like $\beta$ -lactamases Hydrolysis of Carbapenems

Vlatko Stojanoski, Liya Hu, Banumathi Sankaran, Feng Wang,  
Peng Tao, B.V. Venkataram Prasad, and Timothy Palzkill

